Sensors and Materials, Vol. 35, No. 3 (2023) 913–928
MYU Tokyo

S & M 3218

Novel Data Augmentation of Synthetic Aperture Radar Images Based on Angle-InfoGAN Model

Kui Zhang,[1,2] Yanyan Zeng,[1*] Zongxia Xu,[1,2] Hanmei Liang,[1] and Yifei Cao[1]

[1]Beijing Institute of Surveying and Mapping,
No. 15, Yangfangdian Road, Haidian District, Beijing 100038, China
[2]Beijing Key Laboratory of Urban Spatial Information Engineering,
No. 15, Yangfangdian Road, Haidian District, Beijing 100038, China

(Received October 31, 2022; accepted February 13, 2023)

Keywords: data augmentation, Angle-InfoGAN, synthetic aperture radar, template matching, Lee filtering algorithm

Synthetic aperture radar (SAR) has become an important data source in the field of object recognition owing to its high resolution and all-weather characteristics. The traditional data expansion method has difficulty increasing the diversity of samples, which limits the promotion and application of SAR data. Therefore, in view of the shortcomings of traditional SAR data augmentation methods, such as insufficient diversity and poor practicability, we proposed a new idea that can generate samples from different angles. First, Lee filtering and edge direction gradient algorithms are combined to construct a multiscale recursive template matching model, which can identify the target azimuth accurately. Second, we constructed an Angle-Interpretable Representation Learning by Information Maximizing Generative Adversarial Nets (Angle-InfoGAN) model for data generation and extended the original datasets with different new angles. Finally, we applied this method successfully to Moving and Stationary Target Acquisition and Recognition (MSTAR) datasets, and the Fréchet inception distance (FID) was used to compare other data enhancement models to validate the performance of the Angle-InfoGAN model. The samples generated by the Angle-InfoGAN model effectively improve the scale and diversity of SAR image datasets and lay a solid data foundation for deep-learning-based SAR object detection.

1. Introduction

Synthetic aperture radar (SAR) has become an important data source in the field of military and civilian target extraction and identification owing to its high-resolution, all-weather, penetrable cover, especially for use on aircraft and ships. The use of SAR images for automatic target recognition has become an area of research interest in the field of SAR image interpretation.[1,2] In recent years, deep-learning-model-based SAR image target extraction and recognition technologies have active research areas, because they solved the problem that traditional SAR target detection methods can only extract shallow features of images; the use of deep features extracted by deep learning models has greatly improved the accuracy of image

*Corresponding author: e-mail: zengyanyan1989@163.com
https://doi.org/10.18494/SAM4221

ISSN 0914-4935

recognition by SAR. However, the detection of objects by SAR based on deep learning models is not limited by the model structure; too few high-quality samples lead to the overfitting and merging of the model, and the generalization ability of the model is also reduced.

One of the key steps in SAR automatic target recognition (SAR ATR) is feature extraction. Effective features with high separability are obtained from the image to be identified.[3] The typical features of SAR image targets include geometric and texture features, electromagnetic scattering characteristics, and transform domain characteristics. However, in the case of geometric features, owing to the lack of SAR image data sources, sample data corresponding to some key features are lacking; for example, attitude angles of some SAR image objects, such as aircraft and ships, are missing. The issue is how to generate unknown geometric features based on the known geometric features to increase the content of the sample library. In other words, the geometric features of the target (such as the attitude) are used as auxiliary features to generate a sample set at a new angle and thereby improve the accuracy of deep-learning-based SAR image interpretation. Therefore, accurately calculating the angle of the target in the SAR image is a key step in generating high-quality samples, which also affects the accuracy of object recognition.

Image matching is the core task of various computer vision applications and provides new ideas for calculating the azimuthal angle of SAR image targets. Template matching is usually given a template image, and the similarity metric is calculated for the image to be matched to find the region corresponding to the template. This technique is widely used in object tracking, image stitching, medical image analysis, and other fields.[4] Among many classical template matching algorithms, the matching performance of grayscale-based image matching algorithms, such as normalized cross correlation (NCC)[5] and sequence similarity detection algorithm (SSDA),[6] is relatively stable. Therefore, the template matching algorithm can be used to extract geometric features of the SAR target, thereby affecting the quality of the expansion of the dataset.

Currently, two main methods are used to expand SAR datasets: one is the expansion in the geometric space, including the horizontal rotation of the image, random angle flipping, translational rotation, and brightness contrast enhancement. This method is primarily used to expand the data volume of the sample and cannot modify specific features of the object imaged by SAR. The expansion methods in the feature space are mostly based on the variational autoencoder (VAE)[7] and the generative adversarial network (GAN).[8] The training model generates the sample data under the new features, while the GAN includes two modules (a generator and a discriminator), to compare the distribution of the generated image with that of the real image. Compared with VAE, the sample data generated by GAN are closer to the real image, because GAN can input real data into the network model. Hence, GAN is widely used in the field of feature space generation.

In conclusion, to solve the problem of missing SAR target angle features, combined with the superiority of the GAN model in the field of data generation, we proposed a new method for SAR image object angle extraction by combining the Lee filtering and edge direction gradient algorithms. On the basis of the results of extracting the azimuth, an Angle-Interpretable Representation Learning by Information Maximizing Generative Adversarial Nets (Angle-

InfoGAN) model was used to generate samples of multiangle SAR images that can provide high-quality and rich data samples for the recognition and detection of objects from SAR images.

2. Related Work

The accuracy of object recognition based on SAR images depends on the structure of the model, but the fundamental problem is that the sample size is very small, which leads to a low sample diversity. Improving the sample diversity by data augmentation[9] is an effective solution in the case of limited data volume. Data augmentation refers to the expansion of data or the enhancement of features in the original sample datasets with the help of auxiliary data or auxiliary information. Data augmentation adds new data to the original datasets, including horizontal rotation, random angle flip, translation rotation, and brightness contrast enhancement. These methods mainly augment the data volume of the sample but cannot modify the key features of the SAR image target; feature enhancement adds features (such as generating new angles and sizes) to the feature space of the original sample to facilitate image classification by increasing feature diversity.

Sample generation based on feature enhancement has been widely investigated. Commonly used algorithms include the generative adversarial net (GAN). The basic GAN flowchart is shown in Fig. 1. The generator (G) network receives a random noise vector to generate a fake sample, and the discriminator (D) network uses a discriminator to determine the probability of authenticity. The goal is to have the data generated by G to be closer to determine of the real sample.

Mehrotra and Dukkipati[10] applied GAN to small sample learning and proposed a generative adversarial residual pairwise network to solve the single sample learning problem. The algorithm uses a GAN-based generator network to provide an efficient regular representation of invisible data distributions and a residual pairwise network as a discriminator to measure the similarity of paired samples.

The advantage of GAN is sample generation to expand the images of a sample; this method is used in the fields of change detection, target detection, and scene recognition based on the remote sensing images. Lebedev *et al.*[11] conducted a change detection study based on conditional GAN, the accuracy of which was 91%; Rabbi *et al.*[12] achieved the enhancement of

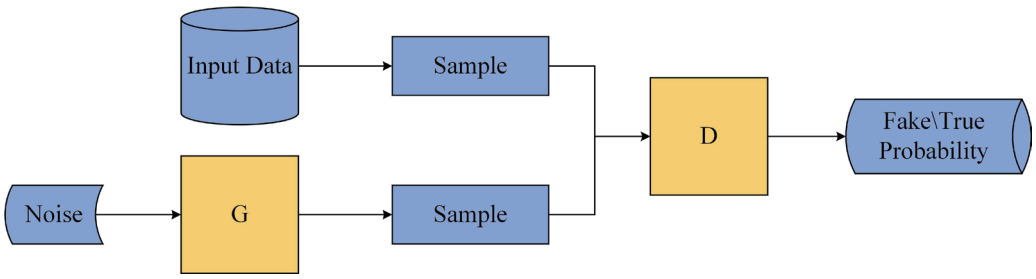

Fig. 1. (Color online) Basic structure chart of GAN, where G and D represent the generator and discriminator networks), respectively.

the remote sensing image quality based on GAN and combined it with the improved faster Region Convolutional Neural Networks (Faster R-CNN) model, and reported an enhancement of the performance of small target detection with an accuracy up to 95.5% on a Cars Overhead With Context (COWC) dataset.

However, these models are only augmented for existing sample data in the field of image generation and still have two drawbacks: (1) they do not capture complex data distributions and (2) they cannot generalize to small sample classes. To solve these problems, Xian *et al.*[13] combined a variational encoder (VAE) and GAN, and took full advantage of both to integrate a new network, F-VAEGAN-D2. This network completed the classification of small sample learning images while representing the feature space. Chen *et al.*[14] continued this study and proposed that the images of the training set could be interpolated to the support set using meta-learning to form an expanded set of support sets.

With the continuous development of GAN models, GAN-based conditional GAN (CGAN), deep convolutional generative adversarial network (DCGAN), Wasserstein GAN (WGAN), and other models have been proposed and widely used in the field of SAR image data generation.[15–18] Guo *et al.*[19] expanded the MSTAR dataset with the original GAN and completed the sample data of SAR targets at each azimuth. Gao *et al.*[20] investigated the effects of different tagging rates on SAR target recognition networks based on DCGAN. The GAN model has been widely applied to the MSTAR dataset and has achieved some results in generating ship data, which confirms the great potential of the GAN model for SAR image data generation. However, these models cannot control the features of sample generation, and the generated features are not interpretable. InfoGAN can change the font size and thickness and angle features of the dataset owing to the incorporation of an implicit vector,[21] so the application of InfoGAN to SAR image targets provides a new method of generating sample data at specific angles.

3. Methods

We proposed a multiangle expansion method for SAR images based on template matching and the Angle-InfoGAN model. The main flowchart is shown in Fig. 2, which includes the following three research methods: 1) Using the template matching and Lee filtering algorithms, more accurate target azimuth information can be obtained to provide a data basis for the training samples required for the production of an accurate Angle-InfoGAN model; 2) the Angle-InfoGAN model can generate multiangle target samples of SAR images, and the results can be used to construct SAR images with a multiangle sample database; and 3) the Frechet inception distance (FID) is used to assess the diversity of samples and to ensure that high-quality samples are generated.

As shown in Fig. 2, the flow of this method is as follows: first, the original SAR datasets are input into the template matching algorithm, the azimuth of each sample is calculated, and the datasets with the azimuth label are created. Second, the datasets are input into the Angle-InfoGAN model to generate samples with different azimuthal angles. Finally, the FID is used to evaluate the quality of samples, and samples with higher quality are stored in the sample library.

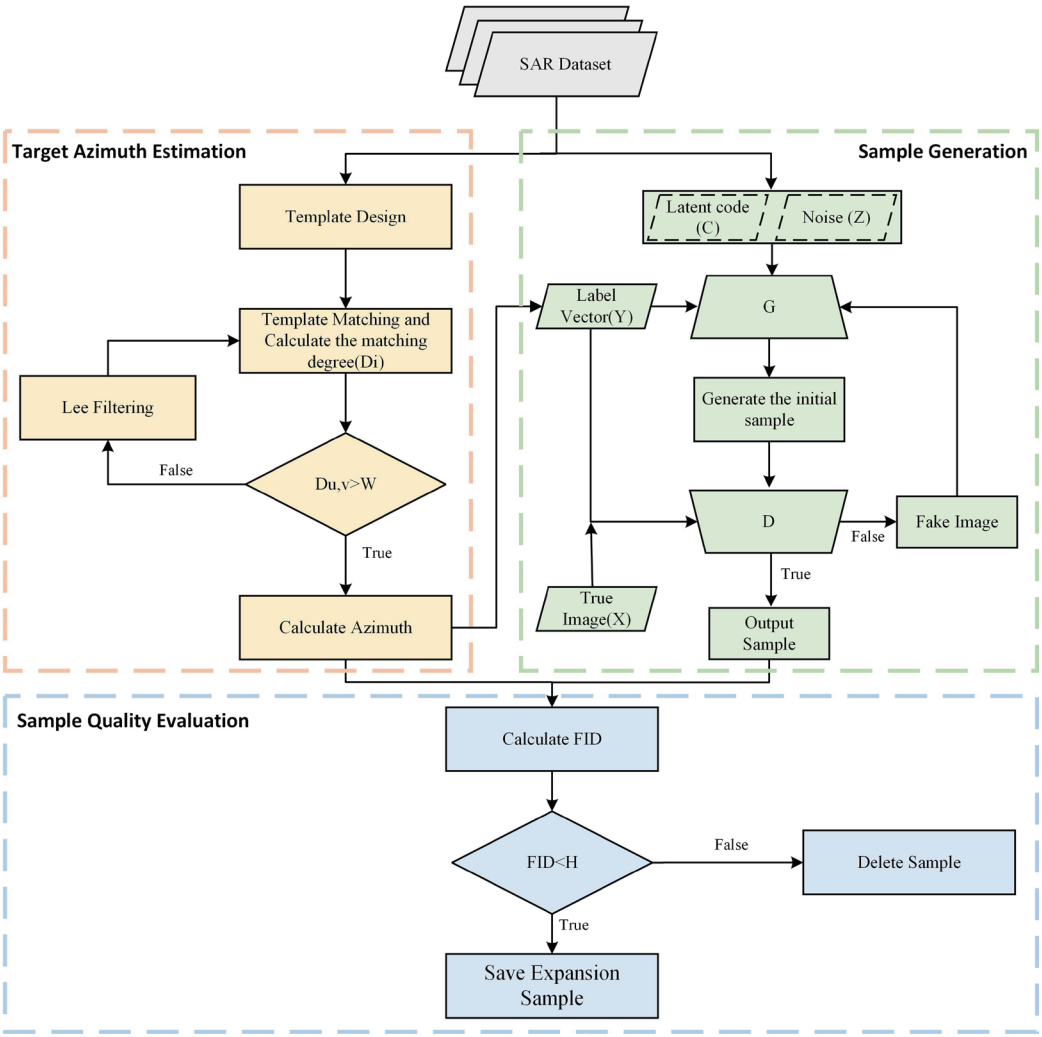

Fig. 2. (Color online) Overall flowchart for the method; $D_{u,v}$ represents the degree of matching.

3.1 Lee filtering algorithm

Lee filtering is a typical method that selects a window with a certain length as a local area and uses the local statistical characteristics of the image to perform SAR image speckle filtering, which is based on a fully developed speckle noise model. Such filtering is a standard deviation-based filtering algorithm that filters the image data according to the statistics (variance coefficient) calculated in a separate window; its mathematical model is

$$F_{ij} = M + K(Y_{i,j} - UM), \tag{1}$$

where $K = UV / (U^2 + M^2 M_{VAR})$ and $M_{VAR} = (S / M)^2$.

3.2 Template matching algorithm based on the edge direction gradient

The template matching algorithm is an image processing method that uses the template target to match the search target when the pose (X, Y, θ) of the target in the searched image is unknown.

The template matching algorithm based on the edge direction gradient should randomly extract an SAR target image from the existing SAR dataset, draw the rectangular frame of the target, crop the image, and input the azimuthal angle of the target as the label (the azimuthal angle of the target is recorded when it points vertically to the north). The image and the azimuth angle label in the rectangular frame are saved as a template. The remaining images are loaded sequentially. The edge direction gradient between the image and the template is calculated to generate the matching degree $D_{u,v}$ of the image, and the matching degree threshold is W. The formula of the template matching algorithm based on the edge direction gradient is

$$D_{u,v} = \frac{1}{n}\sum_{i=1}^{n} \frac{\left(Gx_i^T * Gx_{(u+Xi,v+Yi)}^M\right) + \left(Gy_i^T * Gy_{(u+Xi,v+Yi)}^M\right)}{\sqrt{Gx_i^{T^2} + Gy_i^{T^2}} * \sqrt{Gx_{(u+Xi,v+Yi)}^{M\ 2} + Gy_{(u+Xi,v+Yi)}^{M\ 2}}}, \tag{2}$$

where Gx_i^T and Gy_i^T represent the gradients of the template image (T) in the X and Y directions, and i represents the number of pixels in the image; $Gx_{u,v}^M$ and $Gy_{u,v}^M$ represent the gradients of the image to be matched (M) in the X and Y directions, and u and v represent the row and column numbers of the image to be matched, respectively.

As shown in Fig. 2, the calculated matching degree $D_{u,v}$ is compared with the matching degree threshold W. If it is greater than the threshold, the azimuthal angle A corresponding to the matching result is calculated. After filtering, the matching degree $D_{u,v}$ is recalculated for the filtered image until the azimuthal angle of each image is calculated. The azimuth extraction result of each image is used as the input label of the Angle-InfoGAN model to assist the Angle-InfoGAN model in generating SAR target data in a specific direction.

3.3 SAR data expansion based on Angle-InfoGAN model

In this work, the azimuth results calculated by the methods are sorted into a one-dimensional feature vector, which is recorded as label Y, and the SAR dataset samples are used as the input for the Angle-InfoGAN model. Data samples at different azimuthal angles are generated to solve the problem of missing azimuth angle features in the dataset and effectively to increase the diversity of samples. The general framework of the Angle-InfoGAN model is shown in Fig. 3.

The entire training process is as follows: First, the randomly generated noise vector Z, the label data Y, and the uniformly distributed hidden vector C are combined to construct the feature vector as the input of the G network. The G network returns a fake image, and the fake image and the real image X are input separately. In the D network, the cross-entropy loss function is used to calculate the loss values of the two images, and the two loss values are averaged as the result of the loss calculation of the D network. In the convolution module, according to the cross-entropy loss function of the G network, the parameters of the G network are iteratively updated;

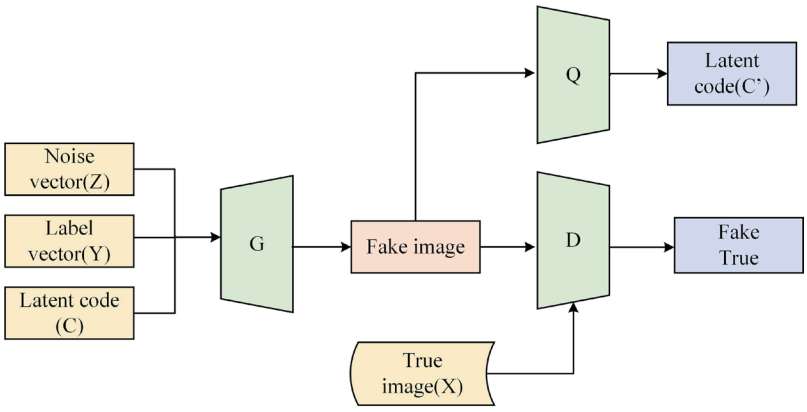

Fig. 3. (Color online) Diagram of general InfoGAN framework.

finally, the fake image is input into the Q network (similar to the structure of the D network model) and two fully connected layers are added to the output module. The parameters of the Q and G networks according to the loss function of the Q network are updated. According to the training process described, the loss function formula of the Angle-InfoGAN model is

$$\min_{G,Q}\max_{D} V_{InfoGAN}(D,G,Q) = V(D,G) - \lambda L_I(G,Q), \tag{3}$$

where $L_I(G,Q)$ represents the regular constraint of mutual information, λ is a hyperparameter, and $V(D,G)$ is the objective function of the inherited generative adversarial network. The equation is and

$$V(D,G) = E_{x\sim p_{data}(x)}\left[\ln D(x)\right] + E_{z\sim p_z(z)}\left[\ln\left(1-D\left(G\left(z\right)\right)\right)\right]. \tag{4}$$

3.4 Evaluation indicators of the sample generation model

For the SAR dataset samples generated by the Angle-InfoGAN model, the FID is used to evaluate both the generated sample and the real sample. The larger the FID, the greater the difference between the two distributions, which is indicated by the Angle-InfoGAN model. There are more samples with new angles in the expanded image, which has a higher diversity. The equation for calculating the FID is

$$FID(x,g) = \left\|\mu_x - \mu_g\right\|_2^2 + Tr\left(\Sigma_x + \Sigma_g - 2\Sigma_x\Sigma_g\right)^{1/2}, \tag{5}$$

where x represents the real image, g represents the image generated by InfoGAN, μ is the mean of the image distribution, and Σ represents the covariance of the image distribution.

On the basis of the FID, the image samples with good results generated by the Angle-InfoGAN model are screened, and the azimuth of each image sample is calculated using the

method described in Sect. 3.2 to continuously increase the diversity of data in the sample database.

4. Experiments and Analysis

The experiments were performed on an Ubuntu 18.04 OS with a CPU (3.4 GHz core i7-6700), RAM (8 GB), and GPU (NVIDIA GTX 2080 8 GB). PyTorch was chosen as the deep learning platform.

4.1 Dataset

The SAR image dataset used in this paper is the Mstar Public Targets Chips, which uses the vehicle dataset in the BTR60 scene. Each image set is a static vehicle image with a pixel size of 128 × 128 obtained by processing the data collected by radar. The angle is in the range of 0–180°, and the target slice images are filtered approximately every 10°. A new data set comprising 935 training patches is created. Some datasets are shown in Fig. 4.

4.2 Target azimuth extraction based on a multiscale recursive template matching model

To obtain more accurate results of the azimuth angle extraction of a vehicle, we combined the edge direction gradient and Lee filtering algorithms. First, vehicle data were selected as the template image; the image when the vehicle target was pointing vertically to the north was selected). When the matching degree calculated by the edge direction gradient algorithm was within the threshold range (the threshold was set to 0.6 in this experiment), the azimuth result obtained by the template matching algorithm was saved, as shown in Fig. 5. The azimuth angle corresponding to each template was created as a training sample.

In Fig. 5, some yellow borders have not been identified. Therefore, we introduced the Lee filtering algorithm. When the matching degree calculated by the edge direction gradient algorithm was less than the threshold, Lee filtering was performed on the image, and the filtered

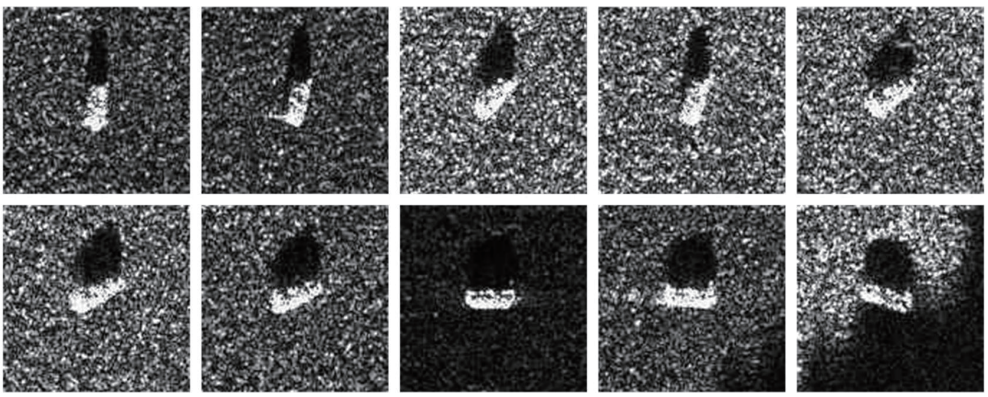

Fig. 4. SAR datasets.

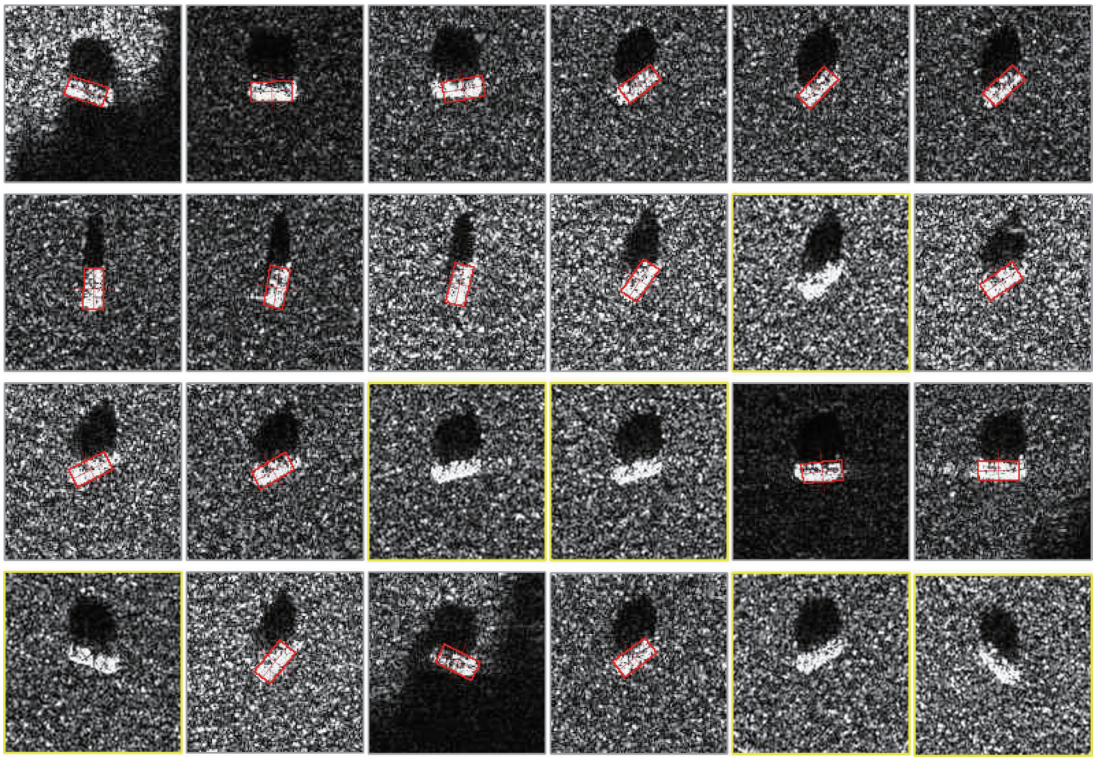

Fig. 5. (Color online) Azimuth angle based on the gradient of the edge direction. The gray boxes represent matched samples; the yellow boxes represent unmatched samples.

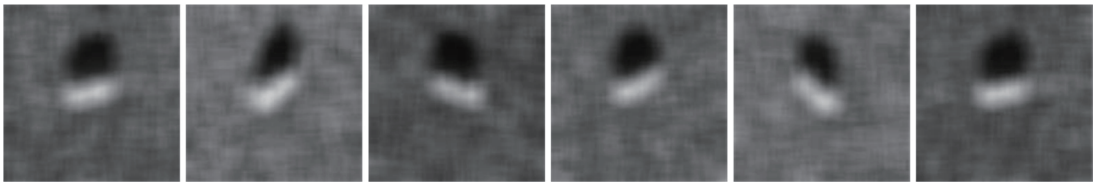

Fig. 6. Results of Lee filtering.

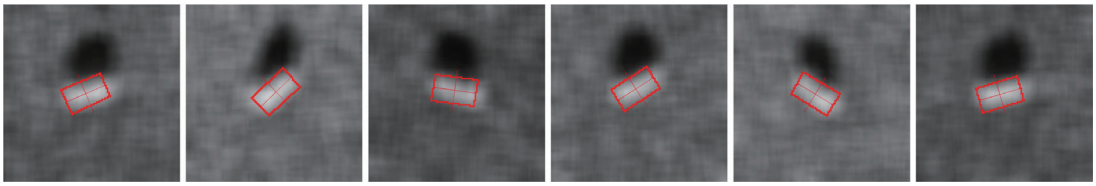

Fig. 7. (Color online) Results of secondary template matching.

image was recalculated. The matching degree was calculated and compared with the threshold, and iterated until the azimuth angle of each vehicle image was calculated. Some filtering results are shown in Fig. 6. Each result was subjected to template matching again to obtain the final azimuthal angle of the target image of each vehicle. The results are shown in Fig. 7.

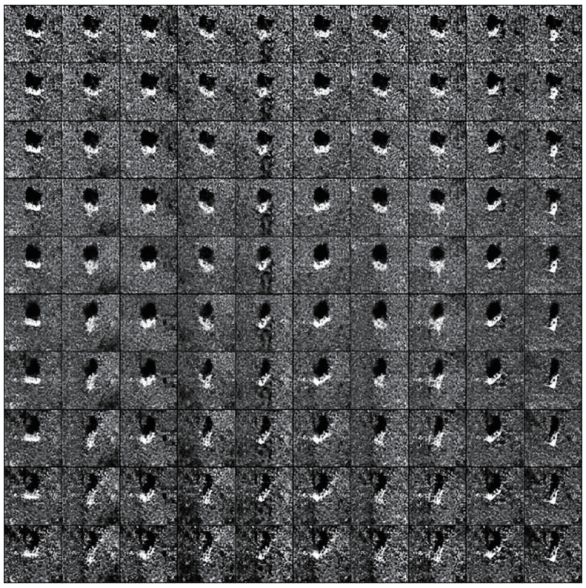

Fig. 8. Overall results of Angle-InfoGAN model (epoch 3000).

4.3 Sample size expansion based on Angle-InfoGAN

We used the Angle-InfoGAN model and compiled the results of epoch 3000 as shown in Fig. 8. From the results of each epoch, the Angle-InfoGAN model continuously updated the angle of sample expansion until epoch 3000 was reached, and we obtained relatively ideal results.

Because the output is a 10 × 10 grid of data, we introduced horizontal and vertical aspects of the images. The horizontal direction shows the results generated from data samples of different vehicles, and the vertical direction refers to the data generated at a specific angle ±5°. From a horizontal perspective, the first result is the result at epoch 0, which shows the initial noise level in the data from the model. At epoch 1000, although some vehicle contours can be generated, they are still affected by considerable noise. In epoch 2000, the vehicle can be basically generated by the model, but the angle of some vehicles is not particularly obvious. In the results of Epoch 3000, the sample vehicle not only has a relatively complete contour but also the sample generated at the new angle is more obvious.

From the longitudinal perspective, there is no obvious angle change between epoch 0 and epoch 1000. Starting from epoch 2000, the angle changes slightly, mainly clockwise or counterclockwise, by ±5°. In epoch 3000, there is basically a change in the angle of each column. The angle range is also basically within ±5°. We used the last column as an example to generate a partial display as shown in Fig. 9.

It can be seen from the above figure that the vehicle gradually shifts clockwise from the angle of 0°, which also proves that our angle label plays a role in the generator and controls the sample generation through the hidden variables.

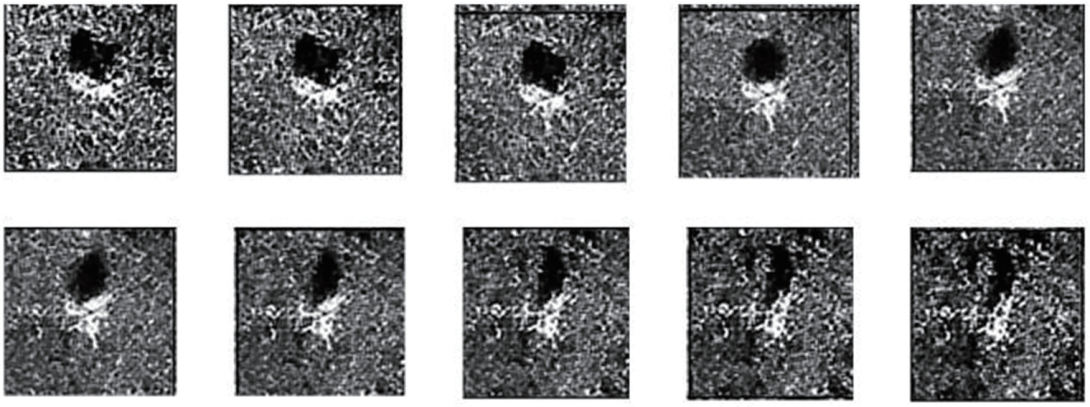

Fig. 9. Local results of Angle-InfoGAN.

4.4 Discussion

4.4.1 Effectiveness of the azimuth extraction algorithm

To verify the effectiveness of template matching based on the edge direction gradient algorithm, we compared and analyzed this algorithm and the grayscale-based template matching algorithm. The edge direction gradient algorithm is a commonly used method in pattern recognition. The idea behind the algorithm is simple, and the algorithm has a high matching accuracy. It is widely used in image matching. Therefore, to verify the effectiveness of the edge direction gradient algorithm proposed, the template matching results obtained by this algorithm were compared with those obtained by the grayscale-based template matching algorithm. The algorithm performed azimuth extraction, and the results are shown in Fig. 10. As can be seen from Fig. 10 (a), only the first data can be used by the grayscale-based algorithm to accurately extract the azimuth angle, but the results in Fig. 10 (b) show that the edge direction gradient algorithm can accurately identify the target, and the extracted azimuth angle is also more accurate with this algorithm. The matching accuracy of the proposed algorithm is 94.8%, while that of the traditional algorithm is 83.2%. Therefore, the azimuth extraction algorithm selected for use in this study was based on the edge direction gradient algorithm.

4.4.2 Performance of the data augmentation model

The Angle-InfoGAN model is used to expand the SAR sample size, and the azimuth angle feature of the target vehicle is used as the hidden vector to control the output of the generator. The diversity of samples provides abundant data for future SAR target recognition. We compared CGAN, WGAN, and InfoGAN without the azimuth angle. To verify the effect of the Angle-InfoGAN model, we showed the results using the same set of data as shown in Fig. 11. In Fig. 11, although the angles of CGAN and WGAN changed regularly, the quality of the generated data is relatively low. The Wasserstein distance was used as the loss function, but the sample data generated are very smooth. Because the angle feature was not used as the hidden vector in

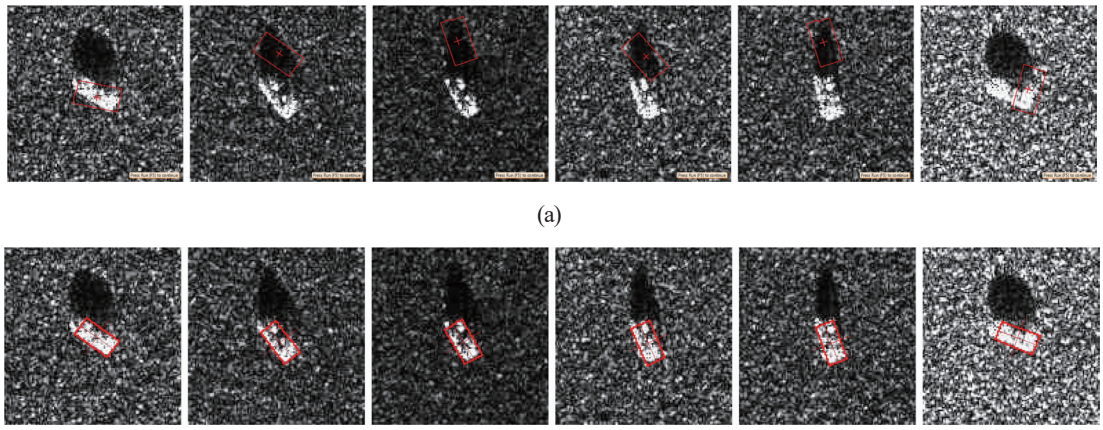

(a)

(b)

Fig. 10. (Color online) Comparison of results of azimuth extraction. (a) Results obtained by the grayscale-based algorithm and (b) results obtained by the edge direction gradient algorithm

the InfoGAN, the sample data at the new angle were not generated. Owing to the addition of the angle characteristics of the target, the data of the unknown angle of the target can be expanded, which meets the demand of increasing the sample diversity.

4.4.3 Performance index evaluation

To better prove the ability of the Angle-InfoGAN model to generate data samples, we use the FID as an indicator to evaluate the performance of the model and compared the FID values of other models. The results of the comparison are shown in Table 1. The FID values of InfoGAN and InfoGAN are the lowest, because the model is not constrained by the angle, and the difference between the results generated and the real sample is the smallest. The FID values of the Angle-InfoGAN, CGAN, and WGAN models all reached 0.6, indicating that these models all generated more samples with new angles, so the difference from the real samples was relatively large, and the FID values were also relatively high. However, among the three models, the FID value of the Angle-InfoGAN model is the smallest, which indicates that the Angle-InfoGAN model not only increases sample diversity but also generates a higher sample quality than the other two models.

4.5 Future work

We can see from Fig. 12 that some problems still arise in sample generation. Although there are changes in the angles of the generated images of this group of samples, the generated images produced some wrong samples owing to the effects of hidden variables. We will address this problem in future work. Different implicit variables will be defined for optimization to meet the requirements of different applications.

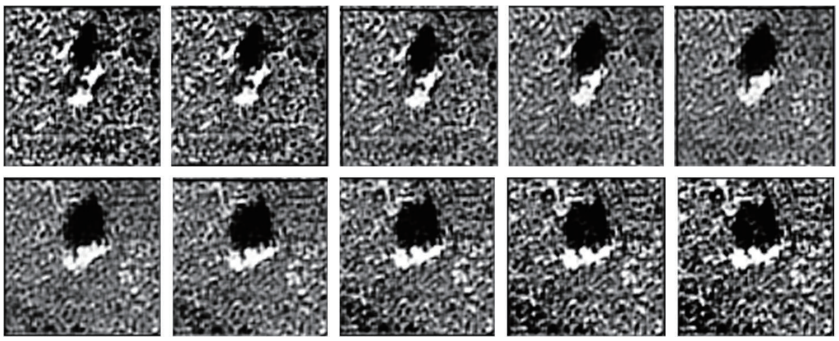

(a)

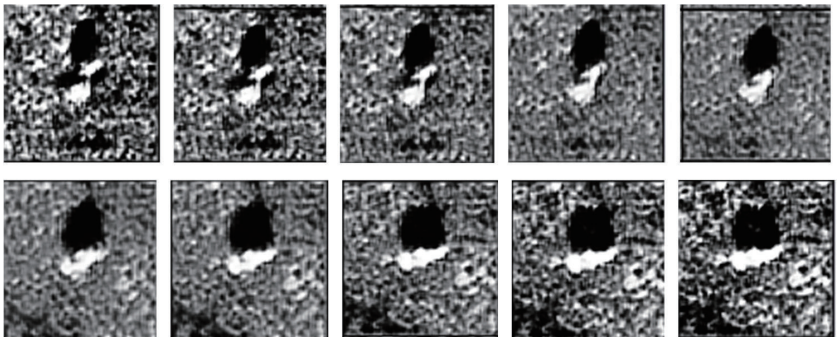

(b)

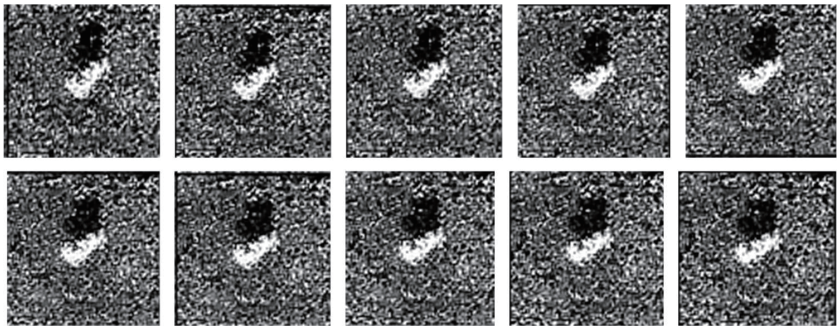

(c)

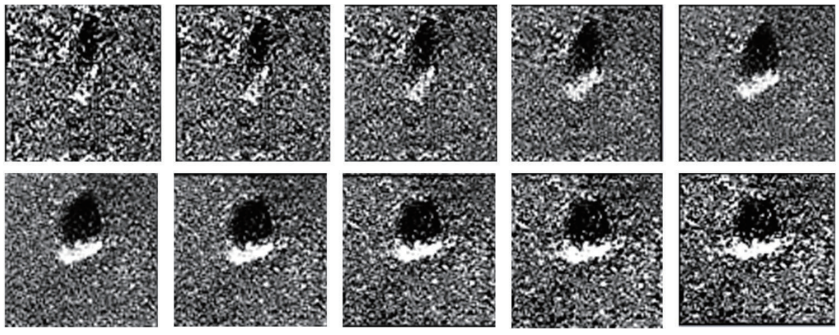

(d)

Fig. 11. Comparison of results of data generation models. (a) CGAN, (b) WGAN, (c) InfoGAN, and (d) Angle-InfoGAN.

Table 1
FID results of performance evaluation.

Model	FID
CGAN	0.637
WGAN	0.653
InfoGAN	0.337
Angle-InfoGAN	0.595

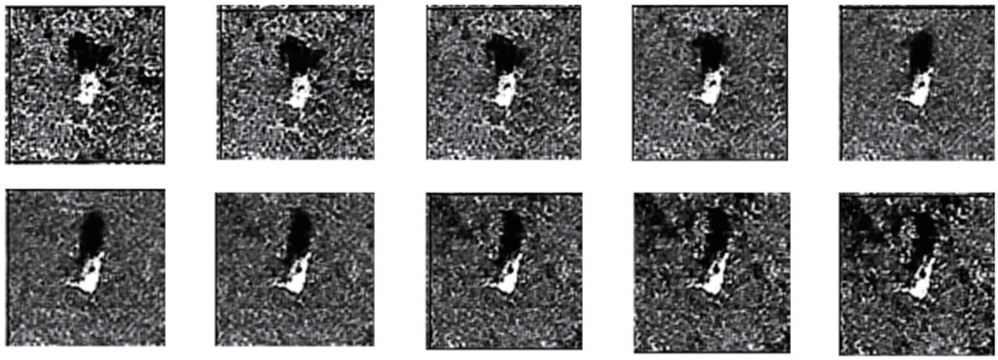

Fig. 12. Error in samples generated by Angle-InfoGAN

5. Conclusions

SAR data augmentation based on the Angle-InfoGAN model can compensate for the lack of SAR sample data, construct a more complete SAR dataset, and promote the development of technology for the interpretation of SAR images. In terms of data expansion, the Angle-InfoGAN model can be better applied in the field of SAR image processing owing to its strong operability and ability to extract more detailed information from real samples to improve the performance of SAR target detection and recognition. In summary, the innovations resulting from this work are as follows: 1) A multiscale recursive template matching model based on the edge direction gradient and filtering algorithms was proposed and the azimuth of each object was accurately calculated model; the extracted results were used as auxiliary features for model input in the Angle-InfoGAN model. 2) An Angle-InfoGAN-based multiangle expansion method for SAR images was proposed. This model attempts to learn interpretable angle features to control the generation of features of SAR image targets. 3) The FID evaluation index was used to obtain high-quality and diverse expansion data and to provide high-quality SAR sample images.

In addition to SAR images, other remote sensing images also lack samples in some areas, resulting in a low accuracy with respect to image classification. The model and idea proposed in this paper can also be adapted to other remote sensing image data, because the input to the Angle-InfoGAN model can be multiband images. In the future, we will conduct experiments on different remote sensing image datasets to improve the quality and diversity of remote sensing image samples, to better assist the detection of objects in images, to detect changes in images, and address other classification tasks.

Acknowledgments

This work was supported by Beijing Key Laboratory of Urban Spatial Information Engineering (No. 2020204) and the task of deep-learning-based research on typical regional change detection technology and application of suspected illegal construction scenarios in Beijing.

References

1 A. Hero, H. Messer, J. Goldberg, D. Thomson, M. Amin, G. Giannakis, A. Swami, J. Tugnait, A. Nehorai, A. Swindlehurst, J. Cardoso, T. Lang, and J. Krolik: IEEE Signal Process Mag. **15** (1998) 21. https://doi.org/10.1109/79.708539
2 P. Forster, P. Larzabal, and E. Boyer: IEEE Trans. Signal Process. **52** (2004) 3183. https://doi.org/10.1109/TSP.2004.836463
3 X. Yang and B. Chen: 12th Int. Conf. Advanced Communication Technology: ICT for Green Growth and Sustainable Development (ICACT 2010) 953–958. https://doi.org/10.3724/SP.J.1146.2009.00515
4 S. Oron, T. Dekel, X. Tian, W. Freeman, and S. Avidan: IEEE Trans. Pattern Anal. Mach. Intell. **40** (2016) 1799. https://doi.org/10.1109/TPAMI.2017.2737424
5 D. Gangodkar, S. Gurbinder, K. Padam, and A. Mittal: Lect. Notes Comput. Sci. (2012) 218. https://doi.org/10.1007/978-3-642-29280-4_26
6 M. Onoe and M. Saito: IEEE Trans. Comput. C **25** (1976) 1052. https://doi.org/10.1109/TC.1976.1674547
7 D. Kingma and M. Welling: Proc. Int. Conf. Learning Representations (2014) 61. https://arxiv.org/pdf/1312.6114.pdf
8 I. Goodfellow, J. Pouget-Abadie, M. Mirza, B. Xu, D. Warde-Farley, S. Ozair, A. Courville, and Y. Bengio: Proc. 27th Int. Conf. Neural Information Processing Systems (2014) 2672. https://dl.acm.org/doi/10.5555/2969033.2969125
9 J. A. Royle, R. M. Dorazio, and W. A. Link: J. Comput. Graphical Stat. **16** (2007) 67. https://doi.org/10.1198/106186007X181425
10 A. Mehrotra and A. Dukkipati: Neural Evol. Comput. (2017) 68. https://doi.org/10.48550/arXiv.1703.08033
11 M. A. Lebedev, Y. V. Vizilter, O. V. Vygolov, V. A. Knyaz, and A. Y. Rubis: Int. Arch. Photogramm. Remote Sens. Spatial Inf. Sci. **42** (2018) 565. https://doi.org/10.5194/isprs-archives-XLII-2-565-2018
12 J. Rabbi, N. Ray, M. Schubert, S. Chowdhury, and D. Chao: Remote Sens. **12** (2020) 1432. https://doi.org/10.3390/rs12091432
13 Y. Xian, S. Sharma, S. Bernt, and A. Zeynep: Proc. IEEE Conf. Computer Vision and Pattern Recognition (2019) 10275. https://doi.org/10.1109/CVPR.2019.01052
14 Z. Chen, Y. Fu, Y. Wang, L. Ma, W. Liu, and M. Hebert: Proc. IEEE Conf. Computer Vision and Pattern Recognition (2019) 8680. https://doi.org/10.1109/CVPR.2019.00888
15 Z. Qin, Z. Liu, P. Zhu, and W. Ling: Comput. Biol. Med. **148** (2022) 1482. https://doi.org/10.1016/j.compbiomed.2022.105928
16 B. Liu, J. Lv, X. Fan, J. Luo, and T. Zou: Mobile Inf. Syst. **2022** (2022) 52. https://doi.org/10.1155/2022/9005552
17 N. Otberdout, M. Daoudi, A. Kacem, L. Ballihi, and S. Berretti: IEEE Trans. Pattern Anal. Mach. Intell. **44** (2022) 848. https://doi.org/10.1109/TPAMI.2020.3002500
18 A. Suryawati, E. Pardede, H. Zilvan, V. Ramdan, A. Krisnandi, D. Heryana, A. Yuwana, R. Kusumo, R. Arisal, A. Supianto, A. Suryawati, E. Pardede, H. Zilvan, V. Ramdan, A. Krisnandi, D. Heryana, A. Yuwana, R. S. Kusumo, R. Budiarianto, A. Supianto, and A. Afif: J. Big Data **8** (2021) 118. https://doi.org/10.1186/s40537-021-00508-9
19 J. Guo, B. Lei, C. Ding, and Y. Zhang: IEEE Geosci. Remote Sens. Lett. **14** (2017) 1111. https://doi.org/10.1109/LGRS.2017.2699196
20 F. Gao, Y. Yang, J. Wang, J. Sun, E. Yang, and H. Zhou: Remote Sens. **10** (2018) 2072. https://doi.org/10.3390/rs10060846
21 X. Chen, Y. Duan, R. Houthooft, J. Schulman, I. Sutskever, and P. Abbeel: Conf. Neural Inf. Process. Syst. (2016) 56. https://doi.org/10.48550/arXiv.1606.03657

About the Authors

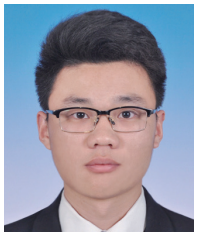

Kui Zhang received his M.S. degree in the School of Information Engineering, China University of Geosciences (Beijing, China) in 2021. He is currently an assistant engineer at the Beijing Institute of Surveying and Mapping, China. He focuses on comprehending SAR images. His specific research interests include data augmentation theory and SAR image information extraction by deep learning methods.(504719347@qq.com)

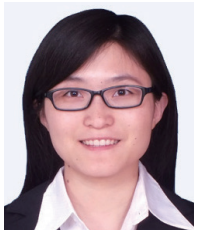

Yanyan Zeng received her B.S. degree from China University of Petroleum, Shandong, China, in 2010 and her Ph. D. degree from the University of Chinese Academy of Sciences, Beijing, China, in 2015. Since 2015, she has been a senior engineer at the Beijing Institute of Surveying and Mapping. Her research interests are in GNSS data processing, new fundamental surveying, and mapping. (zengyanyan1989@163.com)

Zongxia Xu received her master's degree in Geographic Information Engineering from Capital Normal University, China, in 2019. Since 2019, she has been working at the Beijing Institute of Surveying and Mapping, and since 2021, she has been an engineer. Her research interest is in remote sensing image interpretation. (xuzongxia123@163.com)

Hanmei Liang received her master's degree in Human Geography from Capital Normal University, China, in 2012. She served as a college-graduate village official in Daxing District of Beijing from 2012 to 2015 and has been working at the Beijing Institute of Surveying and Mapping since July 2015. Her research interests are in mapping and analyzing geographic information.

Yifei Cao received his B.E. degree in surveying and mapping engineering from Beijing University of Civil Engineering and Architecture, Beijing, China, in 2019 and his master's degree from Beijing University of Civil Engineering and Architecture, China, in 2022. Since 2022, he has been an assistant engineer at the Beijing Institute of Surveying and Mapping, China. His current research interests include object detection and tracking by remote sensing. (1023362448@qq.com)